In-situ Formation of Heterojunctions in Modified Graphitic Carbon Nitride: Synthesis and Noble Metal Free Photo-catalysis

Menny Shalom[†§]*, Miguel Guttentag [‡§], Christian Fettkenhauer[†], Sahika Inal[±], Dieter Neher[±], Antoni Llobet[ɪ], Markus Antonietti[†]

[†]Max-Planck Institute of Colloids and Interfaces, Department of Colloid Chemistry, Research Campus Golm, 14424 Potsdam, Germany

[ɪ] Institut Català d'Investigació Química, Paisos Catalans 16, Tarragona, 43007, Spain

[±]Institute of Physics and Astronomy, University of Potsdam, Karl-Liebknecht-Str. 24-25, Potsdam, 14476, Germany

E-mail address: menny.shalom@ mpikg.mpg.de

Herein we report the facile synthesis of an efficient roll-like carbon nitride (C_3N_4) photocatalyst for hydrogen production using a supramolecular complex composed of cyanuric acid, melamine and barbituric acid as the starting monomers. Optical and photocatalytic investigations show, along with the known red shift of absorption into the visible region, that the insertion of barbituric acid results in the *in situ* formation of in-plane heterojuctions, which enhance the charge separation process under illumination. Moreover, platinum as the standard co-catalyst in photocatalysis could be successfully replaced with first row transition metal-salts and complexes under retention of 50 % of the catalytic activity. Their mode of deposition and interaction with the semiconductor was studied in detail. Utilization of the supramolecular approach opens new opportunities to manipulate charge transfer process within carbon nitride toward the design of more efficient carbon nitride photocatalyst with controlled morphology and optical properties.

1. Introduction

The production of solar fuels through water splitting is highly desired due to the increasing demands for clean and renewable energy.[1] In general, the semiconductor photocatalyst should possess a suitable band gap (< 1.23eV) with the right position of conduction and valence band.[2] In addition, the photocatalytic performance is strongly dependent on the charge transfer processes of the semiconductor under illumination (electrons and holes separation and internal recombination rate). One of the ways to manipulate the charge separation of excitons in many light-driven reactions (*e.g.* in solar cells,[3] light-emitting diodes[4] or for photocatalysis[5]) is the formation of a heterojunction which can be carefully designed in order to direct the charge flow in a given direction. While most of the research in this field was focused on metal-based semiconductors (metal oxides,[6] sulfides[7] and nitrides[8]) as photocatalysts, in the last years metal-free graphitic carbon nitride (C_3N_4) materials have attracted widespread attention due to their outstanding (electro)catalytic and photocatalytic activity.[9] C_3N_4 materials demonstrate high activity in many energy-related fields: as catalyst in heterogeneous catalysis and as metal-free photocatalysts and electrocatalysts in water-splitting reactions,[10, 11] in the degradation of pollutants,[12] and many more. The growing interest in C_3N_4 materials as photo- and electro-catalyst is mainly due to its excellent chemical and photophysical properties. Apart of its high chemical and thermal stability (up to 400°C), energy level positions of C_3N_4 materials are suitable for water splitting under illumination (both proton reduction and water oxidation). The photocatalytic activity of C_3N_4 is strongly dependent on its morphology, size, surface area, defects, and energy states along with its electronic properties (band gap, exciton lifetime *etc.*). In the last year, many modifications of the common synthesis were developed, including the introduction of new heteroatoms (sulfur, phosphor)[13] into the C_3N_4 structure, in order to manipulate its electronic, optical and catalytic properties. However, despite great progress in C_3N_4 synthesis, the traditional solid-state synthesis of C_3N_4 results in disorganized texture, with small grain size and surface defects, which leads to low catalytic activity.

Recently, other groups and ours used the supramolecular chemistry approach to synthesize ordered structures of C_3N_4 such as hollow boxes, spheres and spherical macroscopic assemblies.[12, 14] In addition, this approach can also be applied to grow C_3N_4 on different substrates.[10] Supramolecular chemistry provides a great opportunity for the synthesis of nanostructured materials without any further templating techniques. The supramolecular approach includes the use of non-covalent interactions such as hydrogen bonding to form order between building blocks for the desired synthesis. Hydrogen bonds are very useful for controlling molecular self-assembly thanks to the reversibility, specificity, and directionality of this class of interactions.[15, 16] The structure of the final products can be controlled by choosing the appropriate monomers and solvents for the synthesis. The starting monomers will organize in different structures according to their ability to form hydrogen bonds in the given solvent and form ordered and stable aggregates which consecutively define the resulting materials.

Here we use the supramolecular approach in order to improve the efficiency of the C_3N_4 photocatalyst for hydrogen evolution. The modified carbon nitride was prepared by the pyrolysis of the supramolecular complex of cyanuric acid (C), melamine (M), and barbituric acid (B) as precursors in different molar ratios. We demonstrate that changes in the hydrogen bond network and the replacement of nitrogen atoms with carbon strongly influenced the electronic and the chemical properties of C_3N_4. Moreover, lifetime measurements indicated the *in situ* generation of heterojunctions, which are favorable for photocatalytic applications. The chemical structure, morphology and optical properties of the resulting carbon nitrides were characterized by X-ray diffraction (XRD), Fourier transformed infrared (FT-IR) spectroscopy, scanning electron microscopy (SEM), Elemental Analysis, UV-vis absorption, steady-state and time-resolved fluorescence spectroscopy. The photocatalytic activities of the different modified C_3N_4's were tested by measuring hydrogen evolution in combination with Pt, first row transition metal salts and known water reduction catalysts as co-catalysts.

2. Results and discussion

Supramolecular CM_1B_X complexes were prepared by mixing different molar ratio of the three precursors in water (equimolar amounts of melamine and cyanuric acid = CM_1, x = 0.0033, 0.05, 0.1, 0.5 molar ratio of barbituric acid with respect to CM_1. CM:B = 1:x). Although the

solubility of the three monomers in water is generally low, it was sufficient to allow for the formation of organized aggregates after 4h of shaking (Figure S1). In the absence or in low amounts of barbituric acid (< 0.1) the formation of rod-like aggregates of CMB complex was observed, while in high amount the aggregates in water exhibited a disk-like structure. The change in morphology with higher barbituric acid concentration was probably due to the removal of one hydrogen bond structural unit (when comparing barbituric acid with cyanuric acid), which allowed for more flexibility during the supramolecular complex formation.

Evidence for the formation of high crystallinity supramolecular complexes is given by the FT-IR spectroscopy and XRD analysis (Figure S2).[16] The formation of hydrogen bonds was reflected in the FT-IR spectra by the shift of the stretching vibration of the C=O groups in the cyanuric and barbituric acid from 1691 to 1730 cm^{-1} and by the shift of the triazine ring vibration of melamine to lower wavenumbers (from 812 to 761 cm^{-1}). In addition, the stretching vibration of the N-H group in melamine disappeared. The appearance of new XRD peaks for CMB compared with the starting monomers is strong evidence for the creation of new arrangements (Figure S2b). The indication for an in-plane pattern in CM_1B_x is shown by the well-resolved peaks at 10.7, 19.8 and 21.75°, which can be indexed as (100), (110) and (200) of the in-planar packing, respectively. Photoactive carbon nitride materials were obtained by heating the CMB complexes to 550 °C for 4 hours under nitrogen atmosphere with a heating ramp of 2.3 K/min. The effect of barbituric acid on texture is clearly observed in the SEM images of all CM_1B_X-C_3N_4 samples (Figure 1).
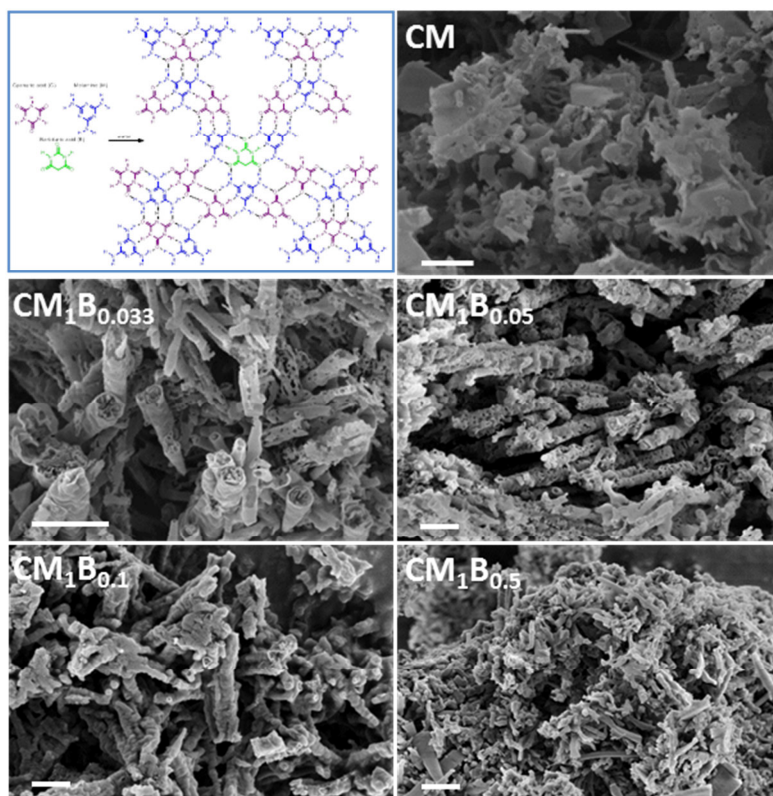
Figure 1. Graphic representation of the CM_1B_x supramolecular complex (see also scheme S1) and SEM images of the hydrogen-bonded complexes CM_1B_x -C_3N_4 in different molar ratios after condensation at 550 °C for 4 hours. Scale bars are 1 µM.

The morphology changed from sheet-like to a roll-like structure, even with low amounts of barbituric acid, due to the local removal of one hydrogen bond. We speculate that the removal of one hydrogen bond introduced more adaptability to the complex by adding more degrees of freedom, which resulted in the ability to create ordered 3D structures. At higher barbituric acid concentration in the starting complex, the roll-like morphology was partially destroyed, and a less regular nanostructured morphology was obtained. This change was also reflected by the BET surface area of all the CM_1B_x-C_3N_4s materials (Figure S3). In the absence and with a low amount of barbituric acid in the starting complex the surface area was relatively high (60-70 m^2 g^{-1}), while its further increase resulted in a surface area decrease. The formation of carbon nitride after heating was confirmed by FT-IR and XRD analyses (Figure 2).[17] The vibrational spectra of the CM_1B_x-C_3N_4 materials were compared to the one that condensed solely from dicyandiamide (DCDA). The strong stretching modes of CN heterocycles from 1200 to 1600 cm^{-1} alongside the characteristic breathing mode of the triazine units at 800 cm^{-1} were observed, confirming the formation of C_3N_4. Additional proof for the C_3N_4 formation is given by the XRD patterns (Figure 2b). The pattern of the carbon

nitride which was condensed from CM_1B_x is similar to the one which was prepared by DCDA condensation. The strong interplanar stacking peak of aromatic systems around 27.2° (indexed as 002) was shifted to lower degrees and became less pronounced and broader with additional barbituric acid. The shift of the interplanar stacking peak can be explained by higher defect rate in the CM_1B_x-C_3N_4s and by the polymer-like growth of CM_1B_x-C_3N_4 compared with the grain-growth in the DCDA route.
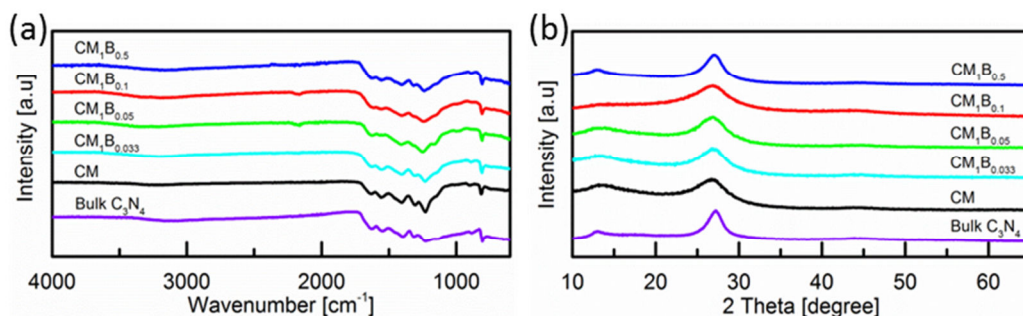

Figure 2. FT-IR spectra (a) and X-ray diffraction pattern (b) of CM_1B_x after condensation at 550 °C for 4 hours, indicating the formation of C_3N_4.

The formation of C_3N_4-like materials was also confirmed by elemental analysis (Table S1). For all the CM_1B_x-C_3N_4 materials, the C/N molar ratio varied from 0.7-0.77 (the increase of carbon content was due to a larger amount of barbituric acid in the starting complex) with ~2% hydrogen only, meaning that most of the NH_2 groups reacted during the condensation process. In addition, the total weight of all the elements clearly indicated the absence of oxygen, implying that most if not all the oxygen from the C=O groups in the cyanuric and barbituric acid were eliminated.

In order to evaluate the changes in the electronic properties of the modified C_3N_4s, we measured their photophysical properties. In general, different morphologies, composition, surface states, and defect sites can directly influence the electronic properties of C_3N_4. The UV-vis diffuse reflectance absorbance spectra of all the CM_1B_x-C_3N_4 materials are shown in Figure 3a. For all the modified CM_1B_x-C_3N_4 materials, the absorption edges were red-shifted to lower energies along with an increase of optical densities at longer wavelengths. The red shift in absorption spectra indicates an alteration of the electronic band structure due to the replacement of nitrogen atoms by carbon atoms, as was previously described by Wang *et al*[18]. Further changes in the electronic properties are shown in the photoluminescence (PL) spectra of the CM_1B_x-C_3N_4 (Figure 3b). As observed in the absorption spectra, the emission

peak of all the CM_1B_X-C_3N_4 materials shifted to lower energy compared to that of the CM-C_3N_4. In addition, the emission intensity is strongly quenched for almost all the CM_1B_X-C_3N_4 materials, probably due to different charge transfer process as will be discussed later.
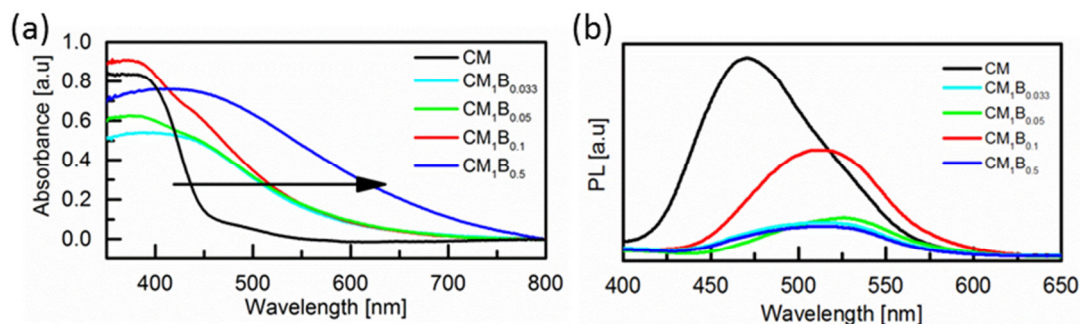


Figure 3. Diffuse reflectance absorption spectra (a) and emission spectra (b) of CM_1B_X-C_3N_4 obtained after condensation at 550 °C for 4 hours.

In order to evaluate the photo-activity of the CM_1B_X-C_3N_4 materials with respect to the bulk and porous C_3N_4, we measured the hydrogen evolution in a water/triethanolamine (TEOA) solution and with Pt as co-catalyst under white light illumination. Considering the low abundance and high cost of platinum, we further conducted a detailed investigation of $CM_1B_{0.05}$ in combination with different known molecular water reduction catalysts (WRCs) and a variety of first row transition metal salts as co-catalysts. In particular detail was investigated the interaction of $CM_1B_{0.05}$ with $Co(BF_4)_2$ and the nature of the catalytic active species in this system.

All of the CM_1B_X-C_3N_4 materials demonstrated higher catalytic activity with Pt as co-catalyst compared to the bulk and CM- C_3N_4. Moreover, the best photocatalyst ($CM_1B_{0.05}$) shows more than 60 % higher turnover frequency (TOF) compared to mesoporous C_3N_4, which is one of the most photo-active C_3N_4 modifications reported up to date. In addition, the photocatalyst demonstrated high stability in the hydrogen evolution reaction, as shown in Figure S4 and S6. The enhanced photocatalytic activity can originate from several factors: (1) better light harvesting which can lead to more charge carriers that can be used in the catalytic process (2) improvement of the charge separation process (with appropriate energy band positioning), and (3) high surface area. From the absorption spectra and the hydrogen production rate it can be estimated that there is no direct correlation between the light harvesting and the photocatalytic activity (e.g. the hydrogen productions of $CM_1B_{0.1}/_{0.5}$ are lower compared to $CM_1B_{0.05}/_{0.01}$ although they absorb higher amount of light). In order to

7

further study the charge separation process, we employed time-resolved fluorescence spectroscopy with a single photon counting set-up[19]. The intensity-averaged fluorescence lifetimes of all the C_3N_4 materials are shown in Figure 4b. In accordance with the trend in the steady-state PL spectra, the fluorescence lifetime decreased for all the CM_1B_x- C_3N_4s compared to CM. The quenching of the emission intensity and its lifetime indicate that the relaxation of a fraction of CM_1B_x-C_3N_4 excited states occurs via non-radiative paths, presumably through charge transfer of electrons and holes to new localized/surface states. Furthermore, for the most active materials, when the monitoring wavelength was changed from 475 nm to 525 nm, the average fluorescence lifetime varied as well, which might point to the presence of more than one type of emitters. The variation of the lifetime suggests that at low barbituric acid concentration the C_3N_4 materials was composed of a distribution of different semiconducting domains with different band gaps (probably due to the low amount of barbituric acid in the starting complex). The *in situ* creation of such domains can form heterojunctions at the grain boundaries, which facilitate the charge transfer processes and consequently enhance the photocatalytic activity (as illustrated in Figure S5).
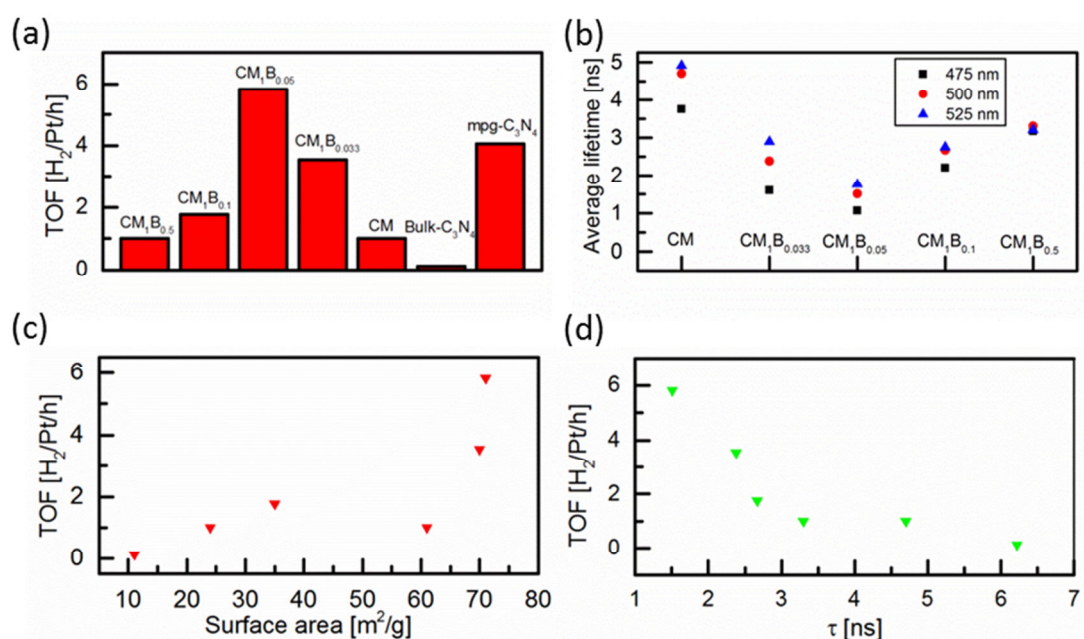
Figure 4. (a) TOFs for different CM_1B_x-C_3N_4s, bulk-C_3N_4 and mesoporous graphitic (mpg)-C_3N_4 under photocatalytic conditions (50 mg g-C_3N_4, 0.21 mM H_2PtCl_6, 10 vol% TEOA, H_2O, total volume 38 ml). (b) Intensity-averaged fluorescence lifetime of CM_1B_x-C_3N_4s; the samples were excited at 405 nm and their emission was monitored at 475, 500 and 525nm. (c+d) TOF versus the surface area and TOF versus the average lifetime. Results are summarized in Table S2.

In order to determine whether the morphology or the electronic properties of the CM_1B_x-C_3N_4 materials are responsible for the photo-activity, the hydrogen evolution rate was plotted as a function of the surface area and the fluorescence lifetime, respectively (Figure 4c and 4d). Although the surface area is related to the materials photo-activity, presumably due to the increase in number of active sites for the reaction, some of the CM_1B_x-C_3N_4 materials exhibit different photo-activity for similar surface areas. Lifetimes, however, clearly correlate with the hydrogen evolution rate, suggesting that the photo-catalytic properties are mainly governed by the electronic structure. This further supports the theory of the formation of heterojunctions, since charge separated states were trapped more efficiently and therefore photocatalytic activity increased with decreasing life time.

In order to replace the platinum co-catalyst, a series of cobalt based WRCs and first row transition metals were tested with $CM_1B_{0.05}$. In a typical standard experiment 3 mL of a degassed, aqueous solution of 10 vol% TEOA, containing 4 mg $CM_1B_{0.05}$ and 0.5 mM of a metal salt or WRC were irradiated with 1 sun of visible light from a xenon lamp (> 400 nm cut off filter) and the evolving hydrogen was detected by means of a Clark electrode. Apart of TEOA other known sacrificial reducing agents were tested (namely ascorbic acid[20], tris-(2-carboxyethyl)phosphine/ascorbic acid[21] and hydroquinone[22]), however, none of those systems produced hydrogen. Figure 5a shows the hydrogen evolution traces for all active co-catalysts including the trace of a blank experiment, where a degased solution of only $CM_1B_{0.05}$ and TEOA was irradiated. Turn over frequencies (TOFs), turnover numbers (TONs) and initialization-time (time between beginning of irradiation and start of H_2 production) for all investigated co-catalysts are summarized in Table S3. While metal salts $Co(BF_4)_2$, $NiAc_2$, and the complex $[CoDOH(H_2O)_2]TFMS_2$ (**S1**)[23] showed catalytic activity, $CuTFMS_2$, $Fe(SO_4)_2$, $ZnCl_2$, $AlTFMS_2$, $[Co^{III}CRCl_2]Cl$ (**S2**)[24] and $[Co^{II}TpyBr_2]$ (**S3**)[25] where inactive towards H_2 production (Scheme S2). In the absence of a suitable co-catalyst the system did not produce any hydrogen. Complex **S1** showed the highest initial rate with an initialization of 2.5 hours, while $Co(BF_4)_2$ performed less efficient but started H_2 production already after 1 hour. $NiAc_2$ was less active than both cobalt species, but started producing hydrogen almost instantaneously after beginning of irradiation. This stands in contrast to a report of Sun et al. When using traditional g-C_3N_4 with Acriflavine as co-photo-sensitizer, nickel salts performed better than their cobalt analogues.[26] The rather surprising complete inactivity of the two well-known WRCs **S2**[24] and **S3**[25] gave a first indication on the mode of interaction between

$CM_1B_{0.05}$ and its co-catalysts (vide infra). Although reduction by the semiconductor should be thermodynamically feasible, neither of the two catalysts produced hydrogen.
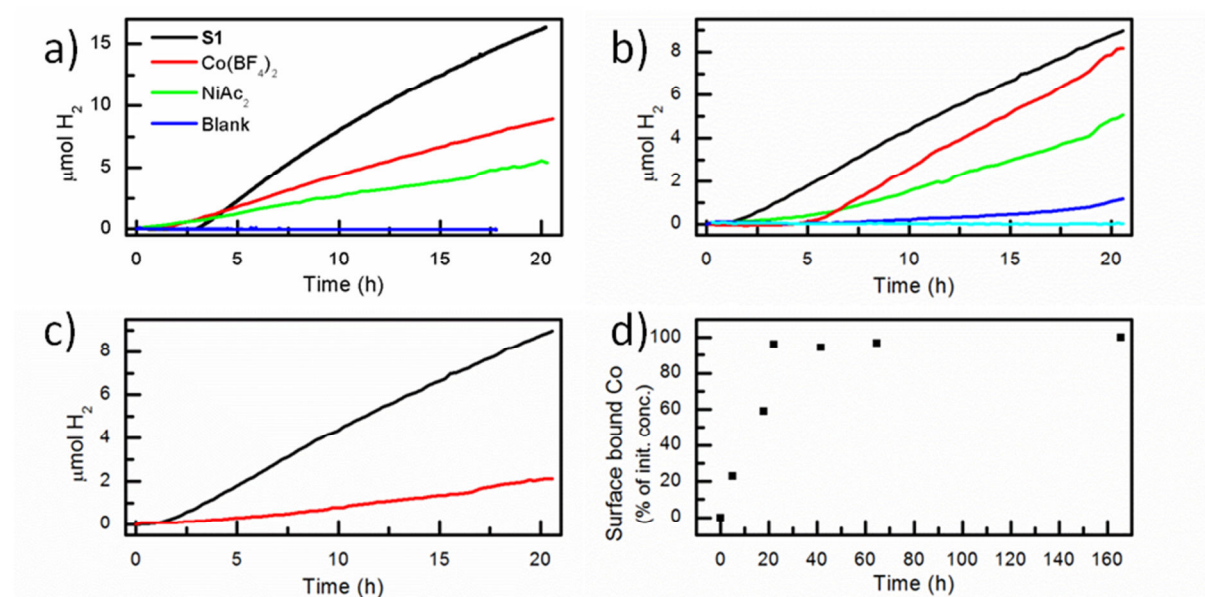

Figure 5. (a) H_2 evolution traces for photo-catalytic experiments with different co-catalysts under standard conditions (4 mg $CM_1B_{0.05}$, 0.5 mM metal salt/ WRC, 10 vol% TEOA, H_2O, total volume 3 mL.) and blank experiment without co-catalyst. (b) H_2 evolution traces for recycle experiments with $Co(BF_4)_2$. Black: typical first run under standard conditions (corresponds to red curve in figure 5a). Green: recycled $CM_1B_{0.05}$ from first run with fresh TEOA solution (10 vol%). Red: recycled $CM_1B_{0.05}$ from first run with fresh TEOA solution (10 vol%) and additional $Co(BF_4)_2$ (0.5 mM). Blue: reuse of the solution from first run after 21 hours of irradiation with fresh $CM_1B_{0.05}$ (4 mg). Cyan: reuse of the solution from first run after 70 hours of irradiation with fresh $CM_1B_{0.05}$ (4 mg). (c) Red: H_2 evolution trace for recycled $CM_1B_{0.05}$ with fresh TEOA solution (10 vol%) after first run was performed in the dark. Black: standard experiment for comparison (corresponds to red curve in figure 5a). (d) Amount of surface bound cobalt, in percentage of initial concentration (0.5 mM), for catalytic experiments under standard conditions stopped after different irradiation times.

In order to understand the nature of the catalytically active species when using $Co(BF_4)_2$ as a co-catalyst, a series of experiments were performed, in which either the solution or the solids where reused for a second photo-catalytic experiment (Figure 5b/c). At first, a catalytic standard solution was centrifuged after one day of irradiation, and the solid was washed and dried. Then, upon addition to a fresh solution of 10 vol% TEOA only, catalytic activity was restored to about 50 % of the original initial rate (Fig. 5b, green). When repeating the procedure, full catalytic activity could be restored when adding additional $Co(BF_4)_2$ to the second run (Fig. 5b, red). When filtering the catalytic solution after one day of irradiation and reusing the filtrate with fresh $CM_1B_{0.05}$, catalytic activity was only restored

10

to a very small extent (Fig. 5b, dark blue). These results strongly indicate a surface bound catalytically active cobalt species. This was further underlined by an experiment, where the first cycle was performed in the dark (1 night, no H_2 detected). After separation from the first catalytic solution and subsequent washing and drying, the solid was used with a fresh solution of TEOA. The material still showed catalytic activity, suggesting the deposition or incorporation of cobalt into the semiconductor even in the absence of photo-induced reducing equivalents (Figure 5c, red).

Since reproducibility of the second runs were in all cases very dependent on the duration of the first run, a sequence of standard experiments were stopped at different reaction times, and the cobalt concentrations of the filtered solutions were determined by ICP measurements. The differences between the initial cobalt concentration and the results from the ICP quantification were assumed to be the amount of metal deposited in some manner on the surface (Figure 5d). Until about 25 hours after start of the reaction, surface cobalt concentration steadily increased up to the point, where all cobalt was bound to the semiconductor. This explained the low but still detectable activity in the second run of the recycle experiment, when fresh $CM_1B_{0.05}$ was added to the filtered catalytic solution, and the not fully restored activity of the recycled $CM_1B_{0.05}$ sample, since in both experiments the catalysis was stopped shortly before reaching complete deposition of the cobalt (small amount of cobalt were still in solution). Therefore, when the first cycle was stopped after 70 hours of irradiation (to ensure complete deposition of the metal) and then reusing the solution with a fresh sample of $CM_1B_{0.05}$, no hydrogen was detected in 1 day of irradiation (Fig. 5b, light blue).

For the other metal salts investigated, the amount of deposited material was determined in the same manner with which the surface cobalt content was established. With the exception of AlTFMS$_2$, all metal ions were deposited on the surface of the semiconductor or somehow incorporated into its framework. The Zn-salt and the Cu-salt almost completely disappeared from the solution, the iron-salt to about 18 %. Nickel was deposited to around 28 % after one day of catalysis. Similar to $Co(BF_4)_2$, it is probably gradually accumulated on $CM_1B_{0.05}$. The same applies for **S1**, which showed around 32 % less cobalt in solution after the same irradiation period (Table S3). The fact that the two highly stable WRCs **S2** and **S3** were inactive towards catalysis, strongly suggests, that mostly deposited material is acting as

active species and that a significant portion of the activity of **S1** is due to its deposited decomposition products undergoing a similar fate as $Co(BF_4)_2$. However, considering the high activity of **S1** and reports of conventional g-C_3N_4 used with similar WRCs the possibility of a homogeneous catalytic contribution cannot be discarded completely.[27, 28]

To further corroborate the presence of cobalt in the solids and as well to determine the nature of the deposition (either in form of nanoparticles or isolated, into the framework of the semiconductor incorporated cobalt ions), SEM-EDX and TEM experiments were performed with the solids before and after catalysis (Figure 6). Although cobalt was found by EDX analysis in the samples from after the catalysis (up to 0.2 mol%, roughly consistent with ICP data), it was not possible to pinpoint the location of the metal. Distribution maps showed evenly dispersed cobalt over the whole of several of the investigated areas. In samples of fresh $CM_1B_{0.05}$ no cobalt was detected. In agreement with the lack of discrete cobalt sites on the surface, no large agglomerates (>5nm) of particles could be found in TEM analysis either, suggesting a mono-atomic distribution of cobalt on or in the semiconductor. In addition, the absence of crystalline cobalt aggregates is also evidenced in the XRD analysis (Figure S7) in which only the typical reflection peaks of C_3N_4 are obtained.[12, 29, 30]
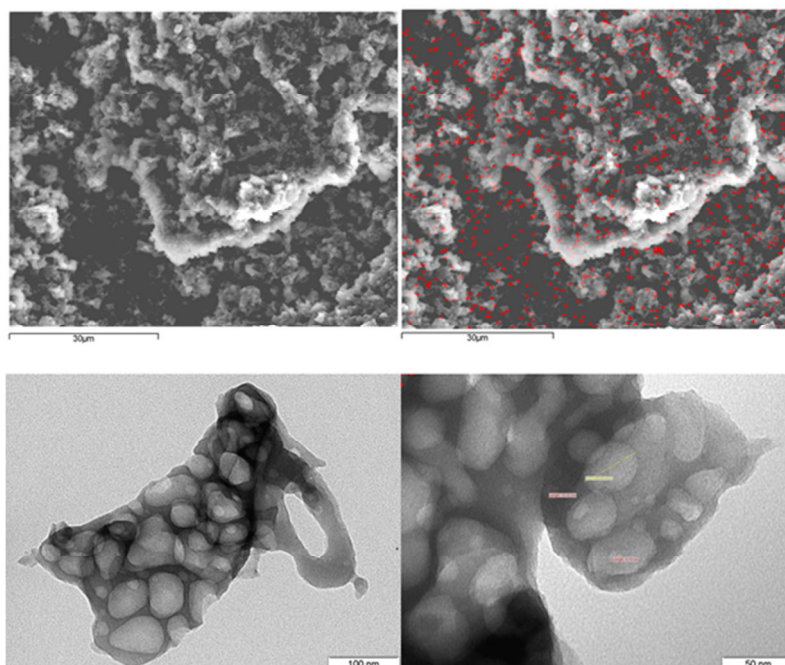
Figure 6. Top: SEM picture of $CM_1B_{0.05}$ after catalysis (left, scale bar 30 µm) and mapping of cobalt according to EDX (right, scale bar 30 µm). Bottom: TEM pictures of $CM_1B_{0.05}$ before (left, scale bar 100 nm) and after (right, scale bar 10 nm) catalysis.

Conclusions

In summary, we demonstrate the synthesis of a highly efficient carbon nitride photocatalyst for hydrogen production by careful design of supramolecular complexes. The resulting $CM_1B_x - C_3N_4$ demonstrates roll-like morphology with different chemical properties. In addition, the insertion of barbituric acid leads to an increase in the optical density along with a red shift into the visible region. The *in situ* formation of heterojunctions (composed from different semiconducting domains) is indirectly evident by life time measurements. The formation of heterojunction improves the charge separation process, resulting in high photocatalytic activity at low barbituric acid concentration. In addition, we also show the successful replacement of platinum as co-catalyst in photo-catalytic hydrogen production by more sustainable transition metals. The system is visible light responsive and performs well without an additional photo-sensitizer or use of UV-light. Co- and Ni-ions and complex **S1** act as co-catalysts for $CM_1B_{0.05}$ for photo-catalytic hydrogen generation. **S1** shows the highest initial rate while $Co(BF_4)_2$ performed better than $NiAc_2$. Recycle experiments and ICP-measurements with $Co(BF_4)_2$ and $CM_1B_{0.05}$ suggest a deposited catalytically active species rather than a homogeneous catalyst. SEM-EDX, TEM and XRD analysis show no evidence for particle formation above 5 nm diameter, further suggesting very small aggregates or a molecular catalytically active species. This work opens the possibility for facile synthetic modification and optimization of C_3N_4 type semiconductors and semiconductor hetero-assemblies, using only earth abundant and low cost starting materials. In addition, the substitution of platinum as co-catalyst with first row transition metals corroborates the importance of the further study of these systems. Lowering the absorption edge further into the visible and improving the interaction between heterogeneous co-catalysts and the material should allow for progressive improvement of photocatalytic efficiencies.

Supporting Information: Experimental details, SEM images, Nitrogen sorption isotherms, FTIR ,XRD and Elemental analysis data along with the structure of the catalysts investigated in this study are given in the supporting information.

AUTHOR INFORMATION

Corresponding Author

Menny.Shalom@mpikg.mpg.de

Author Contributions

§ These authors contributed equally to this work.

Notes

The authors declare no competing financial interest.

REFERENCES

1. H. B. Gray, *Abstr. Pap. Am. Chem. Soc.*, 2013, **246**, 1.
2. K. Maeda and K. Domen, *J. Phys. Chem. Lett.*, 2010, **1**, 2655-2661.
3. M. C. Scharber, D. Wuhlbacher, M. Koppe, P. Denk, C. Waldauf, A. J. Heeger and C. L. Brabec, *Adv. Mater.*, 2006, **18**, 789-+.
4. R. Konenkamp, R. C. Word and M. Godinez, *Nano Lett.*, 2005, **5**, 2005-2008.
5. H. Xu, Y. G. Xu, H. M. Li, J. X. Xia, J. Xiong, S. Yin, C. J. Huang and H. L. Wan, *Dalton T.*, 2012, **41**, 3387-3394.
6. M. Batzill, *Energy Environ. Sci.*, 2011, **4**, 3275-3286.
7. H. J. Yan, J. H. Yang, G. J. Ma, G. P. Wu, X. Zong, Z. B. Lei, J. Y. Shi and C. Li, *J. Catal.*, 2009, **266**, 165-168.
8. A. Kudo and Y. Miseki, *Chem. Soc. Rev.*, 2009, **38**, 253-278.
9. X. C. Wang, K. Maeda, A. Thomas, K. Takanabe, G. Xin, J. M. Carlsson, K. Domen and M. Antonietti, *Nat. Mater.*, 2009, **8**, 76-80.
10. M. Shalom, S. Gimenez, F. Schipper, I. Herraiz-Cardona, J. Bisquert and M. Antonietti, *Angew. Chem.-Int. Edit.*, 2014, **53**, 3654-3658.
11. Y. Zheng, Y. Jiao, J. Chen, J. Liu, J. Liang, A. Du, W. M. Zhang, Z. H. Zhu, S. C. Smith, M. Jaroniec, G. Q. Lu and S. Z. Qiao, *J. Am. Chem. Soc.*, 2011, **133**, 20116-20119.
12. M. Shalom, S. Inal, C. Fettkenhauer, D. Neher and M. Antonietti, *J. Am. Chem. Soc.*, 2013, **135**, 7118-7121.
13. Y. J. Zhang, T. Mori, J. H. Ye and M. Antonietti, *J. Am. Chem. Soc.*, 2010, **132**, 6294-+.
14. J. Young-Si, L. Eun Zoo, W. Xinchen, H. Won Hi, G. D. Stucky and A. Thomas, *Adv. Funct. Mater.*, 2013, **23**, 3661-3667.
15. T. Aida, E. W. Meijer and S. I. Stupp, *Science*, 2012, **335**, 813-817.
16. G. Arrachart, C. Carcel, P. Trens, J. J. E. Moreau and M. W. C. Man, *Chem.-Eur. J.*, 2009, **15**, 6279-6288.
17. B. Jurgens, E. Irran, J. Senker, P. Kroll, H. Muller and W. Schnick, *J. Am. Chem. Soc.*, 2003, **125**, 10288-10300.
18. J. S. Zhang, X. F. Chen, K. Takanabe, K. Maeda, K. Domen, J. D. Epping, X. Z. Fu, M. Antonietti and X. C. Wang, *Angew. Chem.-Int. Edit.*, 2010, **49**, 441-444.
19. J. R. Lakowica, *Springer*, 2009, **3rd ed**

20. M. Guttentag, A. Rodenberg, R. Kopelent, B. Probst, C. Buchwalder, M. Brandstätter, P. Hamm and R. Alberto, *Eur. J. Inorg. Chem.*, 2012, 59-64.
21. C. Bachmann, B. Probst, M. Guttentag and R. Alberto, *Chem. Commun.*, 2014, **50**, 6737-6739.
22. B. Rausch, M. D. Symes and L. Cronin, *J. Am. Chem. Soc.*, 2013, **135**, 13656-13659.
23. B. Probst, M. Guttentag, A. Rodenberg, P. Hamm and R. Alberto, *Inorg. Chem.*, 2011, **50**, 3404-3412.
24. S. Varma, C. E. Castillo, T. Stoll, J. Fortage, A. G. Blackman, F. Molton, A. Deronzier and M. N. Collomb, *Phys. Chem. Chem. Phys.*, 2013, **15**, 17544-17552.
25. M. Guttentag, A. Rodenberg, C. Bachmann, A. Senn, P. Hamm and R. Alberto, *Dalton T.*, 2013, **42**, 334-337.
26. J. F. Dong, M. Wang, X. Q. Li, L. Chen, Y. He and L. C. Sun, *ChemSusChem*, 2012, **5**, 2133-2138.
27. S. W. Cao, X. F. Liu, Y. P. Yuan, Z. Y. Zhang, J. Fang, S. C. J. Loo, J. Barber, T. C. Sum and C. Xue, *Phys. Chem. Chem. Phys.*, 2013, **15**, 18363-18366.
28. L. X., A. J. Ward, A. F. Masters and T. Maschmeyer, *Chem. Eur. J.*, 2014, **20**, 1-7.
29. J. S. Zhang, M. Grzelczak, Y. D. Hou, K. Maeda, K. Domen, X. Z. Fu, M. Antonietti and X. C. Wang, *Chem. Sci.*, 2012, **3**, 443-446.
30. J. T. Jin, X. G. Fu, Q. Liu and J. Y. Zhang, *J. Mater. Chem.*, 2013, **1**, 10538-10545.